


 Cite this: *Nanoscale*, 2023, **15**, 4282

## Self-assembly of $\beta$ -cyclodextrin-pillar[5]arene molecules into supramolecular nanoassemblies: morphology control by stimulus responsiveness and host–guest interactions†

 Jie Lu, Yingying Deng, Peng Liu, Qingqing Han\* and Long Yi Jin \*

Macrocyclic molecules have attracted considerable attention as new functional materials owing to their unique pore size structure and excellent host–guest properties. With the development of macrocyclic compounds, the properties of mono-modified macrocyclic materials can be improved by incorporating pillar[*n*]arene or cyclodextrin derivatives through bridge bonds. Herein, we report the self-assembly of amphiphilic di-macrocyclic host molecules (**H**<sub>1–2</sub>) based on  $\beta$ -cyclodextrin and pillar[5]arene units linked by azophenyl or biphenyl groups. In a H<sub>2</sub>O/DMSO (19 : 1, v/v) mixed polar solvent, an amphiphile **H**<sub>1</sub> with an azophenyl group self-assembled into unique nanorings and exhibited an obvious photoresponsive colour change. This photochromic behaviour makes **H**<sub>1</sub> suitable for application in carbon paper materials on which arbitrary patterns can be erased and rewritten. The amphiphile **H**<sub>2</sub>, with a biphenyl unit, self-assembled into spherical micelles. These differences indicate that various linker units lead to changes in the intermolecular and hydrophilic–hydrophobic interactions. In a CHCl<sub>3</sub>/DMSO (19 : 1, v/v) mixed low-polarity solvent, the amphiphile **H**<sub>1</sub> self-assembled into fibrous aggregates, whereas the molecule **H**<sub>2</sub> assembled into unique nanoring aggregates. In this CHCl<sub>3</sub>/DMSO mixed solvent system, small nanosheet aggregates were formed by the addition of a guest molecule (**G**) composed of tetraphenylethene and hexanenitrile groups. With prolonged aggregation time, the small sheet aggregates further aggregated into cross-linked nanoribbons and eventually formed large nanosheet aggregates. The data reveal that the morphology of **H**<sub>1–2</sub> can be controlled by tuning the intermolecular interactions of the molecules *via* the formation of host–guest complexes. Moreover, the polyhydroxy cyclodextrin unit on **H**<sub>1–2</sub> can be strongly adsorbed on the stationary phase in column chromatography *via* multiple hydrogen bonds, and the singly modified pillar[5]arenes can be successfully separated by host–guest interactions.

Received 18th December 2022,

Accepted 1st February 2023

DOI: 10.1039/d2nr07097a

[rsc.li/nanoscale](http://rsc.li/nanoscale)

## Introduction

Macrocyclic molecules, a class of cyclic molecules with specific pore sizes, have attracted the attention of many chemists and materials scientists in recent years as excellent host molecules in host–guest chemistry.<sup>1–8</sup> Dimacrocyclic host molecules (DHM), as the name suggests, are a type of double host molecule formed by the covalent bridging of two macrocyclic molecules.<sup>9–12</sup> As the host molecules, DHMs not only retain the original host–guest properties of macrocyclic compounds, but also display new properties based on the selection of specific bridging agents. For example, photoresponsive azo-

benzene can be selected as a bridging agent to confer specific photoresponsive properties to the designed materials.<sup>13–19</sup> Different types of macrocyclic molecules can also be selected for bridging to form functional materials.<sup>20</sup> This provides macrocyclic molecules with a more specific recognition ability to form host–guest molecules, leading to more selective separation or recognition properties for the fabrication of functional materials.

Cyclodextrins (CD), which have a hydrophilic outer cavity and hydrophobic inner cavity, are ideal host molecules, similar to enzymes, and have been widely applied in the fields of catalysis, separation, food, and medicine.<sup>21–29</sup> For example, Liu *et al.* constructed hyaluronidase-responsive polysaccharide supramolecular assemblies using chlorambucil,  $\beta$ -CD with hexylimidazolium units, and adamantyl-grafted hyaluronic acid. These aggregates can specifically target cancer cells and respond to hyaluronidase to induce the release of anticancer drugs. Interestingly, the functional  $\beta$ -CD obtained by hydro-

Department of Chemistry, National Demonstration Centre for Experimental Chemistry Education, Yanbian University, Yanji 133002, P. R. China.

E-mail: 000008802@ybu.edu.cn, lyjin@ybu.edu.cn

† Electronic supplementary information (ESI) available. See DOI: <https://doi.org/10.1039/d2nr07097a>

lysis can form a stable 1:1 host-guest complex with ATP, which considerably inhibits the hydrolysis of ATP and cuts off the energy supply of cancer cells, thus effectively alleviating the multidrug resistance of cancer cells.<sup>30</sup> Pillar[*n*]arenes formed by methylene bridges linking *p*-dialkoxy benzene were first reported by Ogoshi in 2008, as a new host family of macrocyclic molecules.<sup>31</sup> Although pillar[*n*]arene molecules have unique columnar structures and specific pore sizes, their poor solubility in water considerably limits their applications in materials science. To overcome these shortcomings, studies have attempted to modify the pillar[*n*]arene matrix *via* different methods to change the properties of pillar[*n*]arenes and expand their application range.<sup>32–38</sup> For example, we previously reported the synthesis and self-assembly of an amphiphilic macromolecule composed of pillar[5]arene, biphenyl, and hydrophilic polyethylene glycol monomethyl ether groups, which can detect aliphatic diamines in aqueous solutions.<sup>39</sup> Huang *et al.* linked crown ethers with pillar[5]arenes through a click reaction, and formed a dynamic rotane with guest molecules through a pH response.<sup>40</sup> However, there are few examples of pillar[*n*]arenes and CD linked together *via* covalent bonds. To the best of our knowledge, only Xin *et al.* used a click reaction to bridge azide-modified  $\alpha$ -CD and pillar[5]arene groups to form hybrid molecules. These molecules can be effectively inserted into a lipid bilayer to form artificial ion channels. As the length of the linker increases, the selectivity of the cation transport changes, where the hybrid molecules with the shortest channel have a specific transmembrane transport preference for K<sup>+</sup>. These results provide a biomimetic alternative to natural K<sup>+</sup> channels.<sup>41</sup> To date, there is no report on the synthesis of molecules based on  $\beta$ -CD and pillar[5]arene units connected by a covalent bond, as a linker.

With this in mind, in this study, we synthesised an amphiphilic  $\beta$ -CD-pillar[5]arene molecule **H**<sub>1</sub> (Scheme 1), which is formed by the linkage of  $\beta$ -CD and pillar[5]arenes through azobenzene. Notably, the azobenzene unit, as a linker, leads to the photoisomerization of **H**<sub>1</sub> for the construction of various

nanostructural aggregates. To investigate the effect of the linker structure on the morphology of the self-assemblies, we also synthesised a molecule **H**<sub>2</sub> containing biphenyl units (Scheme 1). Moreover, sheet-like supramolecular aggregates are constructed from the host-guest complex formed by **H**<sub>1–2</sub> and the guest molecule **G** with a tetraphenylethene group, having strong aggregation-induced emission (AIE) properties.

## Results and discussion

### Synthesis of **H**<sub>1</sub> and **H**<sub>2</sub> and the formation of nanoassemblies in H<sub>2</sub>O/DMSO or CHCl<sub>3</sub>/DMSO

In recent years, bridged pillar[*n*]arene derivatives<sup>42–44</sup> and bridged cyclodextrin derivatives<sup>45–48</sup> have been widely reported for applications in materials science. These molecules are either covalently bridged by two or more pillar[*n*]arene units or covalently bridged by CD units. However, there are few reports of pillar[*n*]arenes and cyclodextrins linked together by covalent bonds. Therefore, amphiphilic molecules **H**<sub>1</sub> and **H**<sub>2</sub> were synthesised by the linkage of  $\beta$ -CD and pillar[5]arene groups using azobenzene or biphenyl, respectively. Molecules **H**<sub>1</sub> and **H**<sub>2</sub> were obtained from a click reaction between an azide-modified  $\beta$ -CD and an azobenzene-functionalized pillar[5]arene or a biphenyl-functionalized pillar[5]arene. The structures of **H**<sub>1</sub> and **H**<sub>2</sub> were characterised using <sup>1</sup>H-NMR and <sup>13</sup>C-NMR spectroscopy (Fig. S27, S28, S29, and S30<sup>†</sup>), elemental analysis, and MALDI-TOF-MS (Fig. S31 and S32<sup>†</sup>). Analysis of the experimental data showed that the molecular structure was consistent with that shown in Scheme 1.

Molecules **H**<sub>1</sub> and **H**<sub>2</sub> are composed of hydrophilic  $\beta$ -CD and hydrophobic rod segments that contain an azobenzene-functionalized pillar[5]arene or a biphenyl-functionalized pillar[5]arene. The strong amphiphilic characteristics of the  $\beta$ -CD unit enable it to exhibit a strong self-assembly behaviour through hydrophilic/hydrophobic interactions in polar solvents, as well as strong hydrogen bonding interactions induced by the large number of hydroxyl groups on  $\beta$ -CD in low-polarity solvents. Therefore, H<sub>2</sub>O/DMSO (v/v = 19 : 1) with high polarity and CHCl<sub>3</sub>/DMSO (v/v = 19 : 1) with low polarity were selected to study the aggregation behaviour of the molecules. Fig. 1 and Fig. S33<sup>†</sup> show the UV-vis and fluorescence (FL) spectra of **H**<sub>1</sub> and **H**<sub>2</sub> in DMSO, H<sub>2</sub>O/DMSO (v/v = 19 : 1), and CHCl<sub>3</sub>/DMSO (v/v = 19 : 1) solutions, respectively ( $3.03 \times 10^{-6}$  mol L<sup>-1</sup>). Compared with that of **H**<sub>1</sub> in DMSO solution, the UV-vis spectra (Fig. 1a and Fig. S33a<sup>†</sup>) of **H**<sub>1</sub> exhibited a blue shift in H<sub>2</sub>O/DMSO and CHCl<sub>3</sub>/DMSO solutions. This indicates that the hydrophobic rod segment of **H**<sub>1</sub> tends to adopt H-type aggregation.<sup>49–51</sup> However, compared with that of **H**<sub>2</sub> in DMSO, the UV-vis spectra (Fig. 1c and Fig. S33c<sup>†</sup>) of **H**<sub>2</sub> exhibited a red shift in H<sub>2</sub>O/DMSO solution and a blue shift in CHCl<sub>3</sub>/DMSO solution. It is proposed that this shift is due to the different dipole moments of the azobenzene and biphenyl units of the **H**<sub>1</sub> and **H**<sub>2</sub> molecules, leading to differences in the strength of the hydrophilic–hydrophobic interactions and steric hindrance of the two molecules. Compared with the



**Scheme 1** Synthesis of **H**<sub>1–2</sub> and the chemical structures of **G**, **H**<sub>3</sub>, and **H**<sub>4</sub>.



**Fig. 1** The absorption spectra of (a)  $H_1$  and (c)  $H_2$ , and emission (excited at 298 nm, Ex bandwidth: 2.5 nm; Em bandwidth: 5 nm) spectra of (b)  $H_1$  and (d)  $H_2$  in DMSO and  $H_2O/DMSO$  ( $v/v = 19:1$ ) solutions ( $3.03 \times 10^{-6} \text{ mol L}^{-1}$ ).

molecules in DMSO solution, obvious fluorescence quenching of  $H_1$  or  $H_2$  was observed in both  $H_2O/DMSO$  and  $CHCl_3/DMSO$  solutions. This further indicates the formation of molecular aggregates in the selected solvents. To determine the size of such aggregates, dynamic light scattering (DLS) data were acquired for the  $H_2O/DMSO$  and  $CHCl_3/DMSO$  solutions of  $H_1$  and  $H_2$ . Molecules  $H_1$  and  $H_2$  formed aggregates with diameters of approximately 21 nm and 20 nm, respectively, in  $H_2O/DMSO$  solution (Fig. S34<sup>†</sup>), and formed aggregates with diameters of approximately 20 nm and 18 nm, respectively, in  $CHCl_3/DMSO$  solution.

Atomic force microscopy (AFM) and transmission electron microscopy (TEM) were used to obtain detailed information about the morphology of the aggregates formed by  $H_1$  and  $H_2$ .  $H_1$  self-aggregated into nanorings with a uniform diameter and width of  $\sim 7$  nm and  $\sim 20$  nm (Fig. 2a and b), respectively,

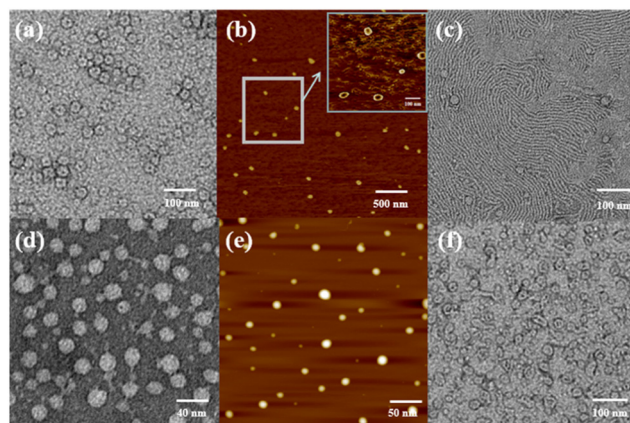


**Fig. 2** The TEM image of (a)  $H_1$  and (d)  $H_2$  and AFM image of (b)  $H_1$  and (e)  $H_2$  obtained from  $3.03 \times 10^{-6} \text{ mol L}^{-1} H_2O/DMSO$  ( $v/v = 19:1$ ) solutions. The TEM image of (c)  $H_1$  and (f)  $H_2$  obtained from  $3.03 \times 10^{-6} \text{ mol L}^{-1} CHCl_3/DMSO$  ( $v/v = 19:1$ ) solution.

in  $H_2O/DMSO$  ( $v/v = 19:1$ ) solutions. Additionally, the full spread length of  $H_1$  was found to be 3.3 nm (Fig. S35a<sup>†</sup>) using CPK modelling, which is consistent with the observed half-diameter. This implies that the rigid hydrophobic segments of  $H_1$  are arranged in a circular shape surrounded by hydrophilic  $\beta$ -CD units to minimise the surface tension of the molecule in aqueous solution (Fig. 3a). Unlike the structure in  $H_2O/DMSO$  solution, in  $CHCl_3/DMSO$  ( $v/v = 19:1$ ) solution,  $H_1$  self-assembled into a nanofibre structure with a diameter of approximately 4.5 nm, which is between one and two times the molecular length when the molecules are fully unfolded. It is proposed that the hydrophilic  $\beta$ -CD units were staggered into rings through hydrogen bonding and surrounded by hydrophobic pillar[5]arene units to minimise the surface tension of the molecules in the  $CHCl_3/DMSO$  solution (Fig. 3b). This may also be due to the weak hydrophilic–hydrophobic interactions of the molecules and stronger hydrogen bond interactions between the  $\beta$ -CD units in the less polar  $CHCl_3/DMSO$  solution. For  $H_2$  with a biphenyl unit as the linker group, the dipole moment is weaker than that of molecule  $H_1$  with azobenzene as the linker unit. Thus,  $H_2$  undergoes weaker hydrophilic–hydrophobic interactions in the  $H_2O/DMSO$  solution with relatively high polarity, leading to assembly into spherical micelles with a diameter of approximately 20 nm, as shown in Fig. 2(d and e). This is considerably longer than the length of 3.1 nm (Fig. S35b<sup>†</sup>) when the molecule is fully unfolded. Thus, in an aqueous solution, the rigid hydrophobic segments of  $H_2$  first aggregate into a nucleus, which is wrapped by hydrophilic  $\beta$ -CD units, and then gradually aggregate to form stable spherical micelles by synergistic driving forces such as hydrogen bonds,  $\pi$ – $\pi$  stacking, and hydrophobic interactions (Fig. 3c). Compared with the azobenzene units, the biphenyl units with weaker dipole moments undergo weaker  $\pi$ – $\pi$  stacking interactions in  $CHCl_3/DMSO$  solution; thus,  $H_2$  was assembled into circular aggregates with a



**Fig. 3** Diagrammatic representation of the self-assembly of molecules  $H_1$  (a and b) and  $H_2$  (c and d) in  $H_2O/DMSO$  and  $CHCl_3/DMSO$  solutions, respectively.

uniform diameter and width of  $\sim 5$  nm and  $\sim 18$  nm (Fig. 2f), respectively. Unlike the assembly arrangement of  $H_1$ , the hydrophilic  $\beta$ -CD units of  $H_2$  are staggered into rings through hydrogen bonding and surrounded by hydrophobic pillar[5] arene units in  $CHCl_3/DMSO$  solution (Fig. 3d).

### Construction of reversible photoresponsive nanostructures of $H_1$ in aqueous solution

The *trans* azobenzene derivatives can form *cis* isomers under ultraviolet (UV) irradiation, which can be restored to the *trans* form upon irradiation with visible light or by increasing the temperature.<sup>52–54</sup> Thus, the photoresponsive properties of  $H_1$  in DMSO solution were initially studied by  $^1H$  NMR spectral analysis. As shown in Fig. 4, the signals of the protons on the azobenzene of the *trans* isomer were shifted upfield, whereas those of the protons on the pillar[5]arene units or  $\beta$ -CD units were not shifted when  $H_1$  was irradiated with 365 nm UV light for 20 min. This is attributed to the photo-induced transformation of the *trans* azobenzene units into the *cis* isomers (*cis*- $H_1$ ). Interestingly, the DMSO solution of  $H_1$  changed from pale-yellow to an orange-yellow solution of *cis*- $H_1$  upon irradiation with UV light (Fig. S36<sup>†</sup>), confirming the occurrence of photoisomerization. UV-vis spectroscopy was used to further examine the photoisomerization of  $H_1$  in  $H_2O/DMSO$  ( $v/v = 19:1$ ) mixed solution. Before UV irradiation, the  $H_2O/DMSO$  solution of  $H_1$  at 25 °C exhibited two characteristic absorption bands (Fig. 5a) at 298 nm and 362 nm, which are related to the  $n-\pi^*$  transitions of the pillar[5]arene units and the  $\pi-\pi^*$  transitions of the *trans* isomers of the azobenzene moieties, respectively. After irradiation with 365 nm UV light, the  $n-\pi^*$  absorption band around 298 nm corresponding to the pillar[5]arene units was almost unchanged; however, a noteworthy decrease in the  $\pi-\pi^*$  absorption band at 362 nm and a new  $n-\pi^*$  absorption band at approximately 450 nm were observed, with a clear isosbestic point at 436 nm (Fig. 5a). This indicates *trans*-to-*cis* isomerisation of the azo-



Fig. 4  $^1H$  NMR spectra (500 MHz,  $DMSO-d_6$ , 25 °C) of (a)  $H_1$  ( $2.72 \times 10^{-3}$  mol  $L^{-1}$ ) and (b)  $H_1$  ( $2.72 \times 10^{-3}$  mol  $L^{-1}$ ) after irradiation with 365 nm UV light for 20 min.



Fig. 5 UV-vis spectra of  $H_1$  in  $H_2O/DMSO$  ( $v/v = 19:1$ ) solution upon exposure to different stimuli: (a) duration of UV irradiation was set to 0–20 min at 365 nm; (b) duration of vis irradiation was set to 0–20 min; (c) different temperatures of  $H_1$  in  $H_2O/DMSO$  ( $v/v = 19:1$ ) solution after 20 min of UV exposure. (d) Absorbance at wavelengths of 362 nm and 450 nm under alternate UV (365 nm) irradiation for 20 min and vis irradiation for 20 min.

benzene units. When the solution of *cis*- $H_1$  was irradiated with visible light, the  $n-\pi^*$  absorption band at 362 nm gradually increased and the  $\pi-\pi^*$  absorption band at 450 nm gradually decreased (Fig. 5b). This phenomenon became more obvious as the visible-light exposure time increased. A similar phenomenon occurred when the solution of *cis*- $H_1$  was heated (Fig. 5c), suggesting *cis*-to-*trans* isomerisation of the azobenzene units. The *trans*-to-*cis* or *cis*-to-*trans* isomerisation was cycled by alternate illumination with 365 nm UV light or visible light (Fig. 5d). Taking advantage of this property of  $H_1$ , as well as the obvious colour change of  $H_1$  shown in Fig. S36<sup>†</sup>, a  $H_2O/DMSO$  solution of  $H_1$  was applied to ordinary copy paper to fabricate photosensitive erasable writing materials. As shown in Fig. S37<sup>†</sup>, the copy paper coated with  $H_1$  was erasable, and specific pictures and text were rewritten with arbitrary patterns.

TEM and AFM were used to intuitively show the effect of UV light on the morphology of the molecular aggregates in solution. Fig. 6 shows the TEM and AFM images of *cis*- $H_1$ . The images show annular aggregates with an outer diameter of



Fig. 6 (a) Negative-staining TEM images and (b) AFM images of *cis*- $H_1$  ( $H_1$  after irradiation with 365 nm UV light for 20 min) obtained from  $3.03 \times 10^{-6}$  mol  $L^{-1}$   $H_2O/DMSO$  ( $v/v = 19:1$ ) solutions. (c) Enlarged image of part b.

approximately 38 nm. The size of the aggregates increased compared with that before illumination (Fig. 2a and b) when the H<sub>2</sub>O/DMSO solution of the dimacrocyclic molecule **H**<sub>1</sub> was irradiated with 365 nm UV light for 20 min. This may result from the synergistic driving force of the molecular arrangement. In this system, the polarity of *cis*-**H**<sub>1</sub> is larger than that of *trans*-**H**<sub>1</sub>, which enhances the hydrophilic–hydrophobic interactions in H<sub>2</sub>O/DMSO solution. In contrast, the increased polarity leads to increased intermolecular force to form a larger-scale arrangement.

### Control of the nanostructures of **H**<sub>1–2</sub> by host–guest complexes

It has been reported that a stable host–guest complex can be formed between alkylnitrile molecules and pillar[5]arene units. Tetraphenyl ethylene, a small organic molecule with AIE properties, has been widely used in advanced materials in recent years owing to its unique luminescence properties.<sup>55–57</sup>

Based on this, we prepared a guest molecule **G** containing tetraphenylethylene and four alkylnitrile units that are strongly associated with pillar[5]arene units. The formation of host–guest complexes between **H**<sub>1–2</sub> and **G** was investigated using <sup>1</sup>H NMR and FL spectroscopy. The above results show that **H**<sub>1</sub> and **H**<sub>2</sub> undergo very strong aggregation in chloroform solution. This induces poor solubility of molecules **H**<sub>1</sub> and **H**<sub>2</sub> in the chloroform solution and limits detailed investigation of the host–guest interaction in chloroform. Furthermore, because the aggregation behaviour leads to weak absorbance of **H**<sub>1</sub> and **H**<sub>2</sub> and fluorescence quenching, it is impossible to determine the association constant of the host–guest complex by UV and fluorescence titration. Therefore, **H**<sub>3</sub> was selected as a model for **H**<sub>1–2</sub> to study the host–guest interaction between the pillar[5]arene unit and alkyl nitrile. In the <sup>1</sup>H NMR spectrum of the chloroform solution of **G** and 4 molar equivalents of **H**<sub>3</sub>, the signals of the H<sub>e,f</sub> protons of **H**<sub>3</sub> were shifted from 6.75 ppm and 3.64 ppm to 6.79 ppm and 3.66 ppm, respectively, whereas the signals of the alkyl H<sub>1–5</sub> protons on molecule **G** were both shifted upfield (Fig. S38†). The shift suggests the formation of a host–guest complex in chloroform. To further confirm this conjecture, <sup>1</sup>H–<sup>1</sup>H NOESY NMR experiments were carried out. As shown in Fig. 7, the H<sub>e,f</sub> protons of **H**<sub>3</sub> and the H<sub>1–5</sub> alkyl protons of **G** were significantly correlated, which indicates that there is a strong host–guest interaction between molecular **H**<sub>3</sub> and **G**. To calculate the value of the association, the equilibrium constant was calculated from the FL titration in CDCl<sub>3</sub> (Fig. S39a†).<sup>58</sup> When the concentration of **G** was 0.05 mM, the fluorescence intensity gradually increased with an increase in **H**<sub>3</sub>. According to the Benesi–Hildebrand equation, the association constant *K*<sub>a</sub> for the interaction of the **G** and **H**<sub>3</sub> molecules was calculated to be 1.22 × 10<sup>17</sup> M<sup>−4</sup> (Fig. S39b†). This higher association constant is reasonable because compound **G** has four recognition sites for complexation. As shown in Fig. S40,† the plot of 1/Δ*X* vs. 1/[host]<sup>4</sup> had a good linear least-squares fit, with a better correlation coefficient compared to that of 1/Δ*X* vs. 1/[host]<sup>*n*</sup> (*n* = 1, 2, 3), indicating that the stoichiometry of the inclusion complex between **H**<sub>3</sub> and compound **G** was 4 : 1. The stoichiometry was also con-



Fig. 7 <sup>1</sup>H–<sup>1</sup>H NOESY NMR spectrum (500 MHz) of the complex of **G** with **H**<sub>3</sub> at a 1 : 4 molar ratio in CDCl<sub>3</sub> at 25 °C.

firmed using the continuous variation method (Job's plot), as shown in Fig. S40.†

Subsequently, **G** molecules were added to **H**<sub>1</sub> and **H**<sub>2</sub>, and the <sup>1</sup>H NMR spectra were recorded to monitor the host–guest interactions in CDCl<sub>3</sub> : DMSO-*d*<sub>6</sub> (v/v = 1 : 1) solution. As shown in Fig. 8 and S41,† the signals of the proton on the benzene ring of the pillar[5]arene unit in **H**<sub>1</sub> or **H**<sub>2</sub> were shifted downfield, and the signals of the alkyl H<sub>1–5</sub> protons on molecule **G** were both shifted upfield. The chemical shift values were consistent with those of molecule **G** in deuterated chloroform solution of **H**<sub>4</sub>, indicating that **H**<sub>1</sub> or **H**<sub>2</sub> and the guest molecule **G** formed complexes through strong host–guest interactions. The signals of the protons on the cyclodextrin unit did not change during this process (Fig. S42†), which further confirmed that a stable 4 : 1 host–guest complex (**H**<sub>1</sub>**C****G** or **H**<sub>2</sub>**C****G**) was formed between the pillar[5]arene unit and the **G** molecule in CHCl<sub>3</sub>/DMSO.

Since the guest molecule **G** itself is an excellent aggregation-induced luminescent material, fluorescence spectroscopy

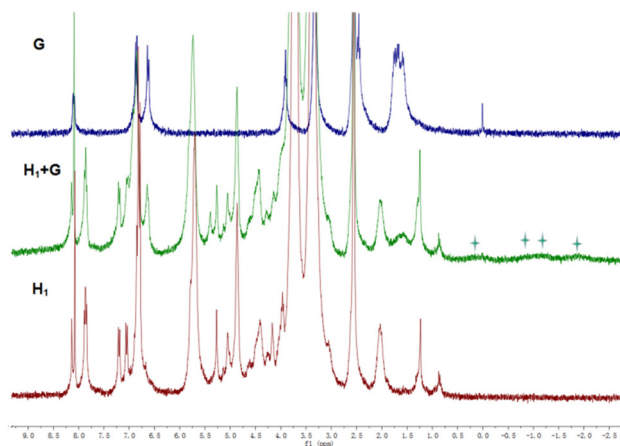


Fig. 8 <sup>1</sup>H NMR spectra of **G** (blue line), **H**<sub>1</sub> + **G** (green line), and **H**<sub>1</sub> (red line) in CDCl<sub>3</sub> : DMSO-*d*<sub>6</sub> (v/v = 1 : 1) at 25 °C.

was used to further verify the formation of the host-guest complex. However, as illustrated in Fig. S43(a),† no obvious fluorescence emission was observed when 1 equiv. of the guest molecule **G** was added to a solution of CHCl<sub>3</sub>/DMSO (v/v = 19 : 1) containing 4 equiv. of **H**<sub>1</sub>. Interestingly, when the guest molecule **G** was added to the solution of CHCl<sub>3</sub>/DMSO (v/v = 19 : 1) of **H**<sub>2</sub>, a strong fluorescence emission peak appeared at 488 nm (Fig. S43b†). This means that **H**<sub>2</sub>**C****G** exhibits strong AIE, compared to **H**<sub>1</sub>**C****G**, which is useful for application in materials science. The fluorescence quenching of **H**<sub>1</sub>**C****G** is attributed to the absorption of the emission of molecule **G** by the photo-responsive azobenzyl group in the **H**<sub>1</sub> molecule, which suppresses the strong fluorescence of the tetraphenylethene unit, consistent with the reports by other groups.<sup>59</sup> To clearly observe such fluorescence changes with the naked eye, 1 equiv. of the guest molecule **G** was added to 4 equiv. of **H**<sub>1</sub> or **H**<sub>2</sub> in CHCl<sub>3</sub>/DMSO (v/v = 5 : 1). Under irradiation with 365 nm ultraviolet light, the solution of **G** presented a weak light-blue fluorescence (Fig. S44†), whereas **H**<sub>1</sub>**C****G** in solution appeared orange-yellow without obvious fluorescence. Interestingly, the **H**<sub>2</sub>**C****G** solution showed bright-white fluorescence when irradiated with UV light, which is consistent with the results of the fluorescence spectroscopy analysis. Notably, the presence of the **H**<sub>1</sub> molecule significantly quenched the fluorescence; thus, this amphiphilic molecule can potentially be used as a sunscreen material.

In order to intuitively demonstrate the influence of the host-guest complex on the aggregate morphology in solution, TEM images of **H**<sub>1</sub>**C****G** and **H**<sub>2</sub>**C****G** were acquired. The experimental data are presented in Fig. 9. When the host-guest complex **H**<sub>1</sub>**C****G** ( $7.58 \times 10^{-7}$  mol L<sup>-1</sup>) was placed in CHCl<sub>3</sub>/DMSO (v/v = 19 : 1) solution for 1 h, an irregular circular small sheet structure with a diameter of approximately 100 nm was observed. When the solution was allowed to stand for 4 h, the aggregate changed from an irregular circular sheet structure to a cross-linked nanoribbon aggregate. After standing for 24 h,

larger nanosheet aggregates were observed. The height of this lamellar aggregate was approximately 7 nm, as measured by AFM (Fig. S45a and c†), which is similar to the sum of the **H**<sub>1</sub> and **G** lengths when the molecules are fully extended (Fig. S35c†). Compared to **H**<sub>1</sub>, which formed nanofibres in CHCl<sub>3</sub>/DMSO, the supramolecular **H**<sub>1</sub>**C****G** molecule composed of rigid pillar[5]arenes and tetraphenylethene through a host-guest interaction undergoes a strong  $\pi$ - $\pi$  stacking interaction to induce the formation of nanosheet-like aggregates with less curvature than the aggregates of **H**<sub>1</sub> in CHCl<sub>3</sub>/DMSO solution. In CHCl<sub>3</sub>/DMSO (v/v = 19 : 1) solution, tetraphenylethene, azobenzene, and the rigid segment of the pillar[5]arenes units are connected by an alkyl nitrile group arranged in the inner sheet through strong  $\pi$ - $\pi$  stacking interactions, and are surrounded by four cyclodextrin units at the outer side of the supramolecule (Fig. 10a).

Similarly, after immersion of the host-guest complex **H**<sub>2</sub>**C****G** ( $7.58 \times 10^{-7}$  mol L<sup>-1</sup>) in CHCl<sub>3</sub>/DMSO (v/v = 19 : 1) solution for 1 h, small nanosheet-like aggregates with a diameter of approximately 50 nm were obtained, where the size was smaller than that of the aggregates of **H**<sub>1</sub>**C****G** (Fig. 9d). We speculate that this is because the linker of **H**<sub>1</sub> contains azobenzene units with a larger dipole moment than that of the biphenyl units. The different driving forces of  $\pi$ - $\pi$  stacking between the two molecules result in slightly different aggregate sizes of the molecules in solution. With an increase in the immersion time to 4 h, cross-linked nanoribbon aggregates were also found (Fig. 9e), and when the immersion time was extended to 24 h, large nanosheet aggregates with a height of ~7 nm (Fig. 9f and S45b and d†) were observed. The experimental results revealed that various nanostructural aggregates can be constructed by the formation of host-guest supramolecular molecules by precisely tuning the intermolecular interactions (Fig. 10b).

In the synthesis of singly modified pillar[5]arene **H**<sub>4</sub>, owing to the excessive addition of *p*-dimethoxybenzene and the low solubility of the by-product **H**<sub>3</sub>, a large amount of the by-product **H**<sub>3</sub> was generated. Since the side-chain bromobutoxy



Fig. 9 TEM images of molecule **H**<sub>1</sub>**C****G** (c/c = 4 : 1) obtained from CHCl<sub>3</sub>/DMSO (v/v = 19 : 1) solutions after (a) 1 h, (b) 4 h and (c) 24 h. TEM images of molecule **H**<sub>2</sub>**C****G** (c/c = 4 : 1) obtained from CHCl<sub>3</sub>/DMSO (v/v = 19 : 1) solution after (d) 1 h, (e) 4 h and (f) 24 h.



Fig. 10 Formation of host-guest complexes (a) **H**<sub>1</sub>**C****G** and (b) **H**<sub>2</sub>**C****G**, and self-assembly in CHCl<sub>3</sub>/DMSO solution, respectively.

group in **H**<sub>4</sub> can form a host–guest complex<sup>60</sup> with **H**<sub>3</sub>, separating these molecules by column chromatography presents challenges. Accordingly, we considered the application of host–guest complexes in the separation of **H**<sub>3</sub> and **H**<sub>4</sub>. Due to the strong intermolecular hydrogen bonds between the multiple hydroxyl units on cyclodextrin and ordinary column chromatography silica gel or neutral aluminium oxide (N-Al<sub>2</sub>O<sub>3</sub>), compounds containing cyclodextrin cannot be separated by ordinary column chromatography using silica gel and N-Al<sub>2</sub>O<sub>3</sub>. Taking advantage of this property, **H**<sub>1</sub> or **H**<sub>2</sub> was thoroughly stirred with N-Al<sub>2</sub>O<sub>3</sub> in DMSO as the stationary phase for column chromatography, and then fully flushed with chloroform solution. After standing for 24 h, a mixture of chloroform and petroleum ether (v/v = 1 : 8) was used to separate the mixture of **H**<sub>3</sub> and **H**<sub>4</sub>. After separation using this chromatographic column, relatively pure **H**<sub>4</sub> was obtained. It is proposed that the effective separation of **H**<sub>3</sub> and **H**<sub>4</sub> was achieved due to the side-chain bromobutoxy group in **H**<sub>4</sub>, which can form host–guest complexes with the pillar[5]arene unit of **H**<sub>1</sub> or **H**<sub>2</sub>. However, for molecule **H**<sub>3</sub>, there is only a weak  $\pi$ – $\pi$  stacking interaction between **H**<sub>3</sub> and **H**<sub>1</sub> or **H**<sub>2</sub>. This interaction is much weaker than the host–guest interaction of **H**<sub>1</sub> or **H**<sub>2</sub>. Infrared (IR) spectroscopy was used to confirm the strong absorption between **H**<sub>1</sub> or **H**<sub>2</sub> and N-Al<sub>2</sub>O<sub>3</sub> (Fig. S46(a)†). Compared with the separated column material, the strength of the stretching vibration peak of the hydroxyl group of **H**<sub>1</sub> decreased, and the absorption peak moved to a lower wavenumber, indicating that **H**<sub>1</sub> interacts with N-Al<sub>2</sub>O<sub>3</sub> by hydrogen bonding. The stationary phase composed of **H**<sub>2</sub> and N-Al<sub>2</sub>O<sub>3</sub> also showed the same phenomenon in the IR tests (Fig. S46(b)†). Thin-layer chromatography (TLC) was used to clarify the separation process. As shown in Fig. S47,† when the TLC plate did not contain **H**<sub>1</sub> or **H**<sub>2</sub>, the *R*<sub>f</sub> values of **H**<sub>3</sub> and **H**<sub>4</sub> were almost the same; however, when the TLC plate contained **H**<sub>1</sub> or **H**<sub>2</sub>, molecules **H**<sub>3</sub> and **H**<sub>4</sub> were separated owing to the host–guest interactions of **H**<sub>1</sub>/**H**<sub>2</sub> and **H**<sub>4</sub>. We believe that this material may be effective for separating molecules such as alkyl amines and halogenated hydrocarbons, which can form host–guest complexes with **H**<sub>1</sub> or **H**<sub>2</sub>.

## Experimental section

Molecules **1**, **2**, **H**<sub>3</sub>, **H**<sub>4</sub>,  $\beta$ -CD-N<sub>3</sub>, and **G** (Scheme 1 and Scheme S1†) were prepared according to previously described methods. All the structural characterisation data are summarised in the ESI (Fig. S1–S32†).

### Synthesis of **H**<sub>1</sub> and **H**<sub>2</sub>

These compounds were synthesised according to the same procedure. The synthesis of **H**<sub>1</sub> is described as a representative example.

**Synthesis of **H**<sub>1</sub>.**  $\beta$ -CD-N<sub>3</sub> (0.101 g, 0.087 mmol) and **1** (0.1 g, 0.096 mmol) were dispersed in 10 ml of DMF and the mixture was degassed. CuSO<sub>4</sub>·5H<sub>2</sub>O (0.024 g, 0.096 mmol) and sodium ascorbate (0.017 g, 0.096 mmol) were added, and the mixture

was heated to 90 °C for 48 h under nitrogen. After DMF was removed, water was added, and the mixture was extracted with dichloromethane. Finally, 0.102 g of the pure target molecule **H**<sub>1</sub> was obtained after purification using Sephadex LH-20.

**Compound **H**<sub>1</sub>.** (Yellow solid, yield: 53.2%, M.p.: 273 °C), <sup>1</sup>H NMR (300 MHz, DMSO-*d*<sub>6</sub>,  $\delta$ , ppm): 8.23 (s, 1H), 7.90–7.84 (m, 4H), 7.24 (d, *J* = 8.4 Hz, 2H), 7.12 (d, *J* = 8.1 Hz, 2H), 6.89–6.75 (m, 10H), 5.93–5.91 (m, 1H), 5.81–5.66 (m, 14H), 5.23–5.17 (m, 2H), 5.07–5.05 (m, 1H), 4.97–4.78 (m, 8H), 4.60–4.46 (m, 6H), 4.36–4.31 (m, 1H), 4.19–4.14 (m, 2H), 4.06–3.51 (m, 73H), 3.17–3.10 (m, 2H), 2.93–2.85 (m, 2H), 1.99–1.87 (m, 4H). <sup>13</sup>C NMR (125 MHz, DMSO-*d*<sub>6</sub>,  $\delta$ , ppm): 161.40, 160.83, 150.44, 150.39, 149.71, 146.84, 146.63, 142.61, 128.00, 127.95, 127.90, 126.05, 124.64, 124.59, 115.72, 115.42, 114.58, 113.81, 102.70, 102.48, 102.36, 101.74, 83.99, 82.58, 82.13, 82.00, 81.93, 81.86, 81.45, 73.71, 73.62, 73.45, 73.34, 73.11, 72.91, 72.83, 72.70, 72.54, 72.34, 70.51, 68.18, 67.83, 61.83, 60.61, 60.55, 60.45, 60.40, 60.32, 59.47, 55.92, 55.88, 55.36, 29.48, 26.27. MALDI-TOF-MS: *m/z* [*M* + Na]<sup>+</sup> 2224.8. Elemental analysis for C<sub>105</sub>H<sub>135</sub>N<sub>5</sub>O<sub>46</sub> (2203.20 g mol<sup>-1</sup>): C: 57.24%, H: 6.18%, N: 3.18%, found: C: 57.18%, H: 6.26%, N: 3.20%.

**Compound **H**<sub>2</sub>.** (White solid, yield: 58.7%, M.p.: 288 °C), <sup>1</sup>H NMR (500 MHz, DMSO-*d*<sub>6</sub>,  $\delta$ , ppm): 8.19 (s, 1H), 7.56–7.55 (m, 4H), 7.11 (d, *J* = 7.5 Hz, 2H), 7.00 (d, *J* = 8.0 Hz, 2H), 6.90–6.70 (m, 10H), 5.90–5.88 (m, 1H), 5.78–5.62 (m, 14H), 5.16–5.11 (m, 2H), 5.06–5.05 (m, 1H), 4.94–4.78 (m, 8H), 4.63–4.46 (m, 6H), 4.33–4.29 (m, 1H), 4.10–4.08 (m, 2H), 4.02–3.99 (m, 2H), 3.92–3.90 (m, 2H), 3.81–3.34 (m, 69H), 3.16–3.12 (m, 2H), 2.93–2.89 (m, 2H), 1.99–1.87 (m, 4H). <sup>13</sup>C NMR (125 MHz, DMSO-*d*<sub>6</sub>,  $\delta$ , ppm): 158.25, 157.75, 150.43, 150.36, 149.70, 143.01, 133.07, 132.69, 128.53, 127.99, 127.94, 127.73, 125.97, 115.55, 115.26, 114.55, 113.78, 102.68, 102.47, 102.36, 101.74, 83.95, 82.54, 82.08, 82.01, 81.91, 81.87, 81.46, 73.70, 73.60, 73.44, 73.33, 73.13, 72.92, 72.84, 72.70, 72.63, 72.24, 70.48, 67.88, 67.74, 61.50, 60.65, 60.49, 60.43, 60.36, 60.32, 59.47, 55.91, 55.84, 55.61, 29.47, 26.21. MALDI-TOF-MS: *m/z* [*M* + Na]<sup>+</sup> 2196.97. Elemental analysis for C<sub>105</sub>H<sub>135</sub>N<sub>3</sub>O<sub>46</sub> (2175.19 g mol<sup>-1</sup>): C: 57.98%, H: 6.26%, N: 1.93%, found: C: 58.06%, H: 6.17%, N: 1.91%.

## Conclusions

Amphiphilic bridged  $\beta$ -cyclodextrin-pillar[5]arene molecules **H**<sub>1</sub> and **H**<sub>2</sub> were successfully synthesised, and their self-assembly behaviour was investigated. Molecule **H**<sub>1</sub> contains a photo-responsive azophenyl group, whereas **H**<sub>2</sub> contains a biphenyl group as a linker. In the H<sub>2</sub>O/DMSO mixed solvent, **H**<sub>1</sub> self-assembled into nanorings, whereas **H**<sub>2</sub> self-assembled into spherical micelles. Similarly, in CHCl<sub>3</sub>/DMSO, **H**<sub>1</sub> self-assembled into fibrous aggregates, whereas **H**<sub>2</sub> assembled into nanoring aggregates, revealing that a slight modification of the chemical structure of the bridging bond can precisely control the morphology of the nanoaggregates. The effect of UV irradiation on the self-assembly of **H**<sub>1</sub> in H<sub>2</sub>O/DMSO solution was investigated. The synergistic interaction between  $\pi$ – $\pi$

stacking and hydrophilic–hydrophobic interactions of **H**<sub>1</sub> in solution led to larger nanoaggregates of *cis*-**H**<sub>1</sub> than those of *trans*-**H**<sub>1</sub> in the H<sub>2</sub>O/DMSO mixed system. Notably, the photo-responsive colour change of **H**<sub>1</sub> enabled its application in carbon paper materials for the fabrication of photosensitive erasable writing materials. Analysis of the self-assembly behaviour of the host–guest complex formed between **H**<sub>1–2</sub> and **G** in CHCl<sub>3</sub>/DMSO solution showed that **H**<sub>1</sub> and **G** form stable host–guest complexes, which assemble into small sheet aggregates under the action of strong hydrogen bonding and  $\pi$ – $\pi$  stacking. With prolonged assembly time, the small sheet aggregates further aggregate into cross-linked nanoribbon aggregates and finally assemble into large sheet aggregates. Similarly, the host–guest complex between **H**<sub>2</sub> and **G** eventually aggregates into large sheet-like aggregates. Notably, because the molecule contains polyhydroxyl  $\beta$ -cyclodextrin units, the molecules can be bound to the neutral alumina filler through hydrogen bonding. Interestingly, the molecular filler can be effectively used in the separation of singly modified pillar[5]arenes from the derivatives of pillar[5]arenes. We expect that these functional molecules will be widely applied in the fields of molecular recognition, sensing, and separation.

## Author contributions

J. Lu: methodology, validation, formal analysis, conducting the experiments, analysis of the experimental results, and writing – original draft. Y. Deng and P. Liu: assisted in the preparation of the molecules. Q. Han: performed the TEM and AFM experiments and analyzed the experimental results. Long Yi Jin: conceptualization, methodology, investigation, resources, supervision, project administration, funding acquisition, and writing – review and editing.

## Conflicts of interest

There are no conflicts to declare.

## Acknowledgements

This work was supported by the National Natural Science Foundation of China (grant numbers 21961041 and 21562043) and the Higher Education Discipline Innovation Project (D18012).

## References

- 1 Y. Mei, Q.-W. Zhang, Q. Gu, Z. Liu, X. He and Y. Tian, *J. Am. Chem. Soc.*, 2022, **144**, 2351–2359.
- 2 H. Zhu, L. Shangguan, D. Xia, J. H. Mondal and B. Shi, *Nanoscale*, 2017, **9**, 8913–8917.
- 3 H. B. Jeon, S. Park, K. R. Ryu, S. K. Ghosh, J. Jung, K. M. Park and J. W. Ha, *Chem. Sci.*, 2021, **12**, 7115–7124.
- 4 Y.-F. Li, Z. Li, Q. Lin and Y.-W. Yang, *Nanoscale*, 2020, **12**, 2180–2200.
- 5 H. Aramoto, M. Osaki, S. Konishi, C. Ueda, Y. Kobayashi, Y. Takashima, A. Harada and H. Yamaguchi, *Chem. Sci.*, 2020, **11**, 4322–4331.
- 6 T. Xiao, L. Xu, L. Zhou, X.-Q. Sun, C. Lin and L. Wang, *J. Mater. Chem. B*, 2019, **7**, 1526–1540.
- 7 C. Tu, W. Wu, W. Liang, D. Zhang, W. Xu, S. Wan, W. Lu and C. Yang, *Angew. Chem., Int. Ed.*, 2022, **61**, e202203541.
- 8 Y.-G. Jia, M. Zhang and X. X. Zhu, *Macromolecules*, 2017, **50**, 9696–9701.
- 9 K.-X. Teng, L.-Y. Niu and Q.-Z. Yang, *Chem. Sci.*, 2022, **13**, 5951–5956.
- 10 H. Li, Y. Yang, F. Xu, Z. Duan, R. Li, H. Wen and W. Tian, *Org. Chem. Front.*, 2021, **8**, 1117–1124.
- 11 H. Kitagishi, S. Kurosawa and K. Kano, *Chem. – Asian J.*, 2016, **11**, 3213–3219.
- 12 Y. Liu, Z. Su, S. Jiang, H. Sun, H. Lyu and Z. Xie, *Polym. Chem.*, 2021, **12**, 6123–6133.
- 13 L. Zhang, J. Gu, X. Luo, Z. Tang, Y. Qu, C. Zhang, H. Liu, J. Liu, C. Xie and Z. Wu, *Nanoscale*, 2022, **14**, 976–983.
- 14 M. Fujiwara, M. Akiyama, M. Hata, K. Shiokawa and R. Nomura, *ACS Nano*, 2008, **2**, 1671–1681.
- 15 L. Dong, Y. Feng, L. Wang and W. Feng, *Chem. Soc. Rev.*, 2018, **47**, 7339–7368.
- 16 M. Zheng and J. Yuan, *Org. Biomol. Chem.*, 2022, **20**, 749–767.
- 17 A. Abdollahi, H. Roghani-Mamaqani, B. Razavi and M. Salami-Kalajahi, *Polym. Chem.*, 2019, **10**, 5686–5720.
- 18 G. K. Joshi, K. N. Blodgett, B. B. Muhoberac, M. A. Johnson, K. A. Smith and R. Sardar, *Nano Lett.*, 2014, **14**, 532–540.
- 19 T. Ogoshi, K. Yoshikoshi, T. Aoki and T.-a. Yamagishi, *Chem. Commun.*, 2013, **49**, 8785–8787.
- 20 X. Yan, D. Xu, J. Chen, M. Zhang, B. Hu, Y. Yu and F. Huang, *Polym. Chem.*, 2013, **4**, 3312–3322.
- 21 L. Yue, H. Ai, Y. Yang, W. Lu and L. Wu, *Chem. Commun.*, 2013, **49**, 9770–9772.
- 22 W. C. E. Schofield, C. D. Bain and J. P. S. Badyal, *Chem. Mater.*, 2012, **24**, 1645–1653.
- 23 F.-F. Shen, Y. Chen, X. Dai, H.-Y. Zhang, B. Zhang, Y. Liu and Y. Liu, *Chem. Sci.*, 2021, **12**, 1851–1857.
- 24 F. Seidi, A. A. Shamsabadi, M. Amini, M. Shabanian and D. Crespy, *Polym. Chem.*, 2019, **10**, 3674–3711.
- 25 S. Datz, B. Illes, D. Gößl, C. v. Schirnding, H. Engelke and T. Bein, *Nanoscale*, 2018, **10**, 16284–16292.
- 26 B. Zhang, W. Guan, S. Zhang, B. Li and L. Wu, *Chem. Commun.*, 2016, **52**, 5308–5311.
- 27 D. J. DeDora, C. Suhrland, S. Goenka, S. M. Chowdhury, G. Lalwani, L. R. Mujica-Parodi and B. Sitharaman, *J. Biomed. Mater. Res., Part B*, 2016, **104**, 1457–1464.
- 28 Z. Liu, W. Zhou, J. Li, H. Zhang, X. Dai, Y. Liu and Y. Liu, *Chem. Sci.*, 2020, **11**, 4791–4800.
- 29 L. Zhou and J. Yu, *J. Sep. Sci.*, 2022, **45**, 2310–2320.
- 30 C. Chen, Y. Chen, X. Dai, J. Li, S. Jia, S. Wang and Y. Liu, *Chem. Commun.*, 2021, **57**, 2812–2815.

- 31 T. Ogoshi, S. Kanai, S. Fujinami, T.-a. Yamagishi and Y. Nakamoto, *J. Am. Chem. Soc.*, 2008, **130**, 5022–5023.
- 32 T. Ogoshi, T.-a. Yamagishi and Y. Nakamoto, *Chem. Rev.*, 2016, **116**, 7937–8002.
- 33 H. Lei, X. Chen, L. Xue, L. Sun, J. Chen, Z. Tan, Z.-G. Zhang, Y. Li and G. Fang, *Nanoscale*, 2018, **10**, 8088–8098.
- 34 Z.-Y. Li, Y. Zhang, C.-W. Zhang, L.-J. Chen, C. Wang, H. Tan, Y. Yu, X. Lo and H.-B. Yang, *J. Am. Chem. Soc.*, 2014, **136**, 8577–8589.
- 35 T. Ogoshi, K. Maruyama, Y. Sakatsume, T. Kakuta, T.-a. Yamagishi, T. Ichikawa and M. Mizuno, *J. Am. Chem. Soc.*, 2019, **141**, 785–789.
- 36 T. Xiao, W. Zhong, L. Xu, X.-Q. Sun, X.-Y. Hu and L. Wang, *Org. Biomol. Chem.*, 2019, **17**, 1336–1350.
- 37 T. Ogoshi, T. Kakuta and T.-a. Yamagishi, *Angew. Chem., Int. Ed.*, 2019, **58**, 2197–2206.
- 38 T. Ogoshi, R. Shiga and T.-a. Yamagishi, *J. Am. Chem. Soc.*, 2012, **134**, 4577–4580.
- 39 J. Lu, X. Gou, Y. Deng, Y.-R. Pei, Z. Huang and L. Y. Jin, *Dyes Pigm.*, 2022, **199**, 110052.
- 40 X. Yan, P. Wei, Z. Li, B. Zheng, S. Dong, F. Huang and Q. Zhou, *Chem. Commun.*, 2013, **49**, 2512–2514.
- 41 P. Xin, H. Kong, Y. Sun, L. Zhao, H. Fang, H. Zhu, T. Jiang, J. Guo, Q. Zhang, W. Dong and C.-P. Chen, *Angew. Chem., Int. Ed.*, 2019, **58**, 2779–2784.
- 42 Y. Cai, X. Yan, S. Wang, Z. Zhu, M. Cen, C. Ou, Q. Zhao, Q. Yan, J. Wang and Y. Yao, *Inorg. Chem.*, 2021, **60**, 2883–2887.
- 43 Y. Wang, M.-Z. Lv, N. Song, Z.-J. Liu, C. Wang and Y.-W. Yang, *Macromolecules*, 2017, **50**, 5759–5766.
- 44 S. Sun, X.-Y. Hu, D. Chen, J. Shi, Y. Dong, C. Lin, Y. Pan and L. Wang, *Polym. Chem.*, 2013, **4**, 2224–2229.
- 45 X. Dai, X. Dong, Z. Liu, G. Liu and Y. Liu, *Biomacromolecules*, 2020, **21**, 5369–5379.
- 46 Y. Liu, Y. Chen, L. Li, H. Y. Zhang, S. X. Liu and X. D. Guan, *J. Org. Chem.*, 2001, **66**, 8518–8527.
- 47 Y. Liu, G.-S. Chen, L. Li, H.-Y. Zhang, D.-X. Cao and Y.-J. Yuan, *J. Med. Chem.*, 2003, **46**, 4634–4637.
- 48 X. Guan, D. Zhang, T. Jia, Y. Zhang, L. Meng, Q. Jin, H. Ma, D. Lu, S. Lai and Z. Lei, *Ind. Eng. Chem. Res.*, 2017, **56**, 3913–3919.
- 49 N. Ye, Y.-r. Pei, Q. Han, M. Lee and L. Y. Jin, *Soft Matter*, 2021, **17**, 6661–6668.
- 50 S. Yu, R. Shan, G.-Y. Sun, T. Chen, L. Wu and L. Y. Jin, *ACS Appl. Mater. Interfaces*, 2018, **10**, 22529–22536.
- 51 J. Lu, Y. Deng, K. Zhong, Z. Huang and L. Y. Jin, *Polym. Int.*, 2022, **71**, 478–486.
- 52 S. Yu, T. Yang, M. Sui, G.-Y. Sun, T. Chen and L. Y. Jin, *Dyes Pigm.*, 2019, **171**, 107694.
- 53 S. Qian, S. Li, W. Xiong, H. Khan, J. Huang and W. Zhang, *Polym. Chem.*, 2019, **10**, 5001–5009.
- 54 A. Adam and G. Haberhauer, *J. Am. Chem. Soc.*, 2017, **139**, 9708–9713.
- 55 G. Zhang, B. Li, Y. Zhou, X. Chen, B. Li, Z.-Y. Lu and L. Wu, *Nat. Commun.*, 2020, **11**, 425.
- 56 S. Wang, Y. Wang, Z. Chen, Y. Lin, L. Weng, K. Han, J. Li, X. Jia and C. Li, *Chem. Commun.*, 2015, **51**, 3434–3437.
- 57 N. Song, D.-X. Chen, Y.-C. Qiu, X.-Y. Yang, B. Xu, W. Tian and Y.-W. Yang, *Chem. Commun.*, 2014, **50**, 8231–8234.
- 58 H. Zhang, K. T. Nguyen, X. Ma, H. Yan, J. Guo, L. Zhu and Y. Zhao, *Org. Biomol. Chem.*, 2013, **11**, 2070–2074.
- 59 R. Arumugaperumal, W.-L. Hua, P. Raghunath, M.-C. Lin and W.-S. Chung, *ACS Appl. Mater. Interfaces*, 2020, **12**, 29650–29660.
- 60 X. Wang, K. Han, J. Li, X. Jia and C. Li, *Polym. Chem.*, 2013, **4**, 3998–4003.